INTERNATIONAL JOURNAL OF CLIMATOLOGY
Int. J. Climatol. **22**: 1267–1284 (2002)
Published online in Wiley InterScience (www.interscience.wiley.com). DOI: 10.1002/joc.774

PARAMETERIZATION OF EFFECTIVE ICE PARTICLE SIZE FOR HIGH-LATITUDE CLOUDS

FAISAL S. BOUDALA,[a,b,*] GEORGE A. ISAAC,[a,b] QIANG FU[a,c] and STEWART G. COBER[b]

[a] *Department of Oceanography, Dalhousie University, Halifax, Nova Scotia B3H 4J1, Canada*
[b] *Meteorological Service of Canada, Toronto, Ontario M3H 5T4, Canada*
[c] *Department of Atmospheric Sciences, University of Washington, Seattle, WA 98195-1640, USA*

Received 15 August 2001
Revised 19 December 2001
Accepted 6 January 2002

ABSTRACT

A parameterization has been developed for mean effective size D_{ge} in terms of ice water content (IWC) and temperature using *in situ* measurements of ice crystal spectra, cloud particle shapes and particle cross-sectional area A from four research projects conducted in latitudes north of 45 °N. The cloud microphysical measurements were made using PMS 2D optical probes, a PMS forward scattering spectrometer probe (FSSP), and Nevzorov total water and liquid water content probes. The IWCs derived from particle spectra using three different methods were compared with IWC measured with the Nevzorov probe (IWC_{Nev}). The contribution of small particles to the total mass was estimated by integrating a gamma distribution function that was fitted to match the measured FSSP concentrations. The D_{ge} was calculated from the derived IWC and total cross-sectional area per unit volume A_c.

This analysis indicates that there are significant differences among the schemes used to derive the IWC. It was found that the IWC derived based on the Cunningham scheme and IWC_{Nev} have the highest correlation: $r^2 = 0.78$. After considering small particles, the derived IWC almost matched the IWC_{Nev}. The average estimated contribution of small particles to the A_c was 43%. The average estimated contribution of small particles to the total IWC, however, was 20%. Since D_{ge} is directly proportional to the ratio IWC/A_c, the addition of small particles reduced the derived D_{ge} considerably. The largest changes in D_{ge} associated with small particles, however, occur at the coldest temperature and at low IWC, reaching up to 45% for temperatures less than −25 °C. Generally, D_{ge} and IWC increase with increasing temperature. Good agreement between the parameterized D_{ge} and derived D_{ge} from measurements were found when small particles were included. Copyright © 2002 Royal Meteorological Society.

KEY WORDS: effective sizes of ice crystals; high latitude; stratiform ice clouds; parameterization in climate models; ice water content; small ice crystal; cross-sectional area per unit volume of ice crystals; application in radiation models

1. INTRODUCTION

Satellite observations and general circulation model (GCM) studies suggest that ice clouds have an important impact on the Earth's climate by influencing the radiation balance and hydrological cycle (Ramanathan *et al*., 1983; Ramaswamy and Ramanathan, 1989). Intercomparisons of several GCMs have shown that the models have problems in simulating the current climate, particularly in the polar regions (Boer *et al*., 1992). One problem is partly caused by the fact that GCM simulations are performed without incorporating realistic values of the single scattering properties (SSP) of ice clouds in the cloud radiation parameterizations.

The important microphysical parameters used to describe the SSP of ice clouds are the ice water content (IWC) and the effective size of the ice crystals (Sun and Shine, 1995; Fu, 1996; Fu *et al*., 1998). Sun and Shine (1995) used IWC to parameterize the SSP of ice clouds, and assumed that the IWC implicitly contained the ice particle size. This assumption requires further investigation. Fu (1996) and Fu *et al*. (1998) defined a

* Correspondence to: Faisal S. Boudala, Meteorological Service of Canada, Cloud Physics Research Division, Downsview, Ontario, M3H 5T4, Canada; e-mail: Boudala.Faisal@ec.gc.ca

mean effective size D_{ge} of non-spherical ice crystals in terms of IWC and total projected area per unit volume A_c (see Equation (6)). Then the extinction coefficient β, asymmetry factor g, and single scattering albedo ω are parameterized in terms of D_{ge} and IWC. For the solar spectrum, an improved geometric optics method (GOM) (Yang and Liou, 1996a) that was valid for size parameter $\chi \geq 15$ was used (Fu, 1996). The parameter χ is defined as $\chi = \pi D / \lambda$, where λ is the wavelength of light and D is the size of the ice particle. For the infrared spectrum, a composite scheme, including GOM, Mie, and the finite difference time domain (FDTD) (Yang and Liou, 1996b) techniques, has been applied (Fu *et al.*, 1998). Such simplified schemes can be used to calculate SSP of ice clouds in a GCM with an accuracy comparable to the exact methods, albeit with less computer time.

Though GCMs predict IWC, they do not simulate particle size distributions. Most GCMs use a globally fixed effective size for ice clouds. Therefore, there is a need for parameterization of SSP of ice clouds in terms of GCM-predicted variables such as IWC and temperature. There are some studies of these parameters in tropical (Heymsfield and MacFarquhar, 1996; MacFarquhar and Heymsfield, 1997) and mid-latitude cirrus (Heymsfield and Platt, 1984) clouds. For example, MacFarquhar and Heymsfield (1997) and Heymsfield and Platt (1984) parameterized ice crystal size distributions in terms of temperature and IWC. Thus, for a given IWC and temperature, which may be predicted from climate models, the effective ice crystal sizes can be calculated by integrating the size distribution. However, similar studies are not available in high-latitude stratiform ice clouds. Also, the parameterization of mean effective size is very dependent on the accuracy of the IWC determination. The IWC has been determined from measured A and particle size distributions (e.g. Heymsfield and Platt, 1984; McFarquhar and Heymsfield, 1998). However, the methods have not been adequately validated against direct *in situ* measurements.

In this study, IWC, derived using three different schemes are tested against the IWC measurements made with a Nevzorov total water content (TWC) probe (Korolev *et al.*, 1998b). Then, derived D_{ge} is parameterized in terms of IWC and temperature T. The parameterizations are done with and without small particles and are suitable for climate modelling applications.

2. MEASUREMENTS OF CLOUD MICROPHYSICAL PARAMETERS

2.1. Field projects

The data were collected during four projects, which are described below. The National Research Council (NRC) Convair-580 aircraft was used in all four projects. The Beaufort and Arctic Storms Experiment (BASE) field project was conducted in October 1994 over the Canadian western Arctic. It was designed to study weather conditions in the Beaufort Sea and other surrounding areas of the Arctic (Hudak *et al.*, 1996; Gultepe *et al.*, 2000). The FIRE Arctic Cloud Experiment (FIRE.ACE) project began in April 1998 and ended in July 1998, with the Convair-580 measurements being made in April. The scientific objectives of FIRE.ACE were to study the impact of Arctic clouds on the radiation exchange between the surface and the atmosphere (Curry *et al.*, 2000). The Canadian Freezing Drizzle Experiment I (CFDE I) project was conducted in March 1995 over Newfoundland and the Atlantic Ocean. The Canadian Freezing Drizzle Experiment III (CFDE III) started in December 1997 and ended in February 1998. During the CFDE III project, the aircraft flew over southern Ontario and Quebec, Lake Ontario and Lake Erie. These two projects were aimed at studying aircraft icing in winter storms, but a significant fraction of the clouds encountered were glaciated (Cober *et al.*, 2001; Isaac *et al.*, 2001).

2.2. Instrumentation

The types of instrumentation used in these projects are described in Isaac *et al.* (2001). The calibrations of the instruments and processing of the data are described in Cober *et al.* (2001). The instruments used in this work are the PMS FSSP, 2D-C, 2D-P probes, as well as the Nevzorov liquid water content (LWC) and TWC probes.

Korolev *et al*. (1998b) describe the Nevzorov TWC/LWC probe. The probe has two separate sensors (hot wires), one for TWC and the other for LWC measurements. Comparison measurements made with Nevzorov and similar types of probe in high-speed wind-tunnel experiments suggest that the probe can measure LWC and TWC within an accuracy of 15% and the sensitivity of the instrument is estimated to be in the range of 0.003 to 0.005 g m^{-3}.

The forward scattering spectrometer probe (FSSP) was designed to measure sizes and concentrations of spherical particles. Extensive discussions about the accuracy and performance of this probe can be found in Baumgardner and Spowart (1990), Brenguier (1989), and Wendisch *et al*. (1996). It is believed that the spherical particle sizes are measured within ±20% and concentration is measured within ±17% (Baumgardner, 1983). The probe has been used to estimate concentrations of ice particles (Gardiner and Hallett, 1985; Strapp *et al*., 1999; Arnott *et al*., 2000; Gultepe *et al*., 2001). In the presence of irregular ice crystals, Gardiner and Hallett (1985) reported that the FSSP measured ice concentrations were two to three orders of magnitude higher than those derived from a replicator. However, a recent study by Arnott *et al*. (2000) suggests that the replicator underestimates the concentration of particles ($D < 50$ μm). Therefore, the FSSP may not overestimate particle concentrations by two to three orders of magnitude as suggested by Gardiner and Hallett (1985). In fact, the FSSP may give reasonable estimates of ice particles concentration in some glaciated clouds (Strapp *et al*., 1999; Gultepe *et al*., 2001).

The PMS 2D probe was developed by Knollenberg (1970). The 2D-C and 2D-P probes measure concentrations in the particle size ranges of 25–800 μm and 200–6400 μm respectively. However, the first four channels of 2D-C have been ignored here because of the measurement uncertainty (Korolev *et al*., 1998a). The 2D-C images were processed following a *centre-in* scheme. This scheme includes all partly imaged particles that have their centres within the sampling area. Their sizes are determined by reconstruction of their shapes assuming circular geometry (Heymsfield and Parrish, 1978). The 2D-P images are processed following an *entire-in* scheme (Knollenberg, 1970). This method is based on ignoring any particle that occludes either end of the photodiode array and it is also referred as the double edge element (DEE).

2.3. Cloud phase segregation

Both the cloud particle habits recognition technique, based on several geometric ratio tests applied to the 2D images, and the phase segregation scheme are described in Cober *et al*. (2001). They showed that glaciated clouds are generally characterized by fractions of circular images <0.35 on the 2D probes. In addition, all glaciated clouds are generally characterized by Nevzorov LWC/TWC ratios of <0.25 and FSSP concentrations of <15 cm^{-3}. In this study, all three conditions are applied to identify glaciated clouds, and 30 s averaged data were used.

3. DERIVED IWC FROM 2D-C AND 2D-P MEASUREMENTS

3.1. Derivation of the IWC

The IWC is usually derived from 2D-C and 2D-P measurements using either scheme

$$\mathrm{IWC} = \frac{4}{3}\pi\rho\mathrm{w}\sum_{ij} N_{ij}(D_{\mathrm{e}ij}/2)^3 \tag{1a}$$

or

$$\mathrm{IWC} = \sum_{ij} N_{ij} M_{ij} \tag{1b}$$

where N_{ij} is the concentration of ice particles in a given bin size i and habit j, and ρw is the density of water, $D_{\mathrm{e}ij}$ is the equivalent melted diameter for given i and j, M_{ij} is the mass of particle with size i and

habit j. The two latter quantities have been determined by the following two relationships:

$$M_{ij} = a_j D_{ij}^{b_j} \tag{2a}$$

$$D_{eij} = a_j A_{ij}^{b_j} \tag{2b}$$

where D_{ij} is the maximum dimension of the ice particles, A_{ij} is the projected area and a and b are some constants for a given habit j. To examine the accuracy/usefulness of obtaining derived IWC from ice particle spectra measured using 2D-C and 2D-P probes, particle images were categorized according to their maximum length and mean maximum length (as the mean of the maximum chord lengths measured parallel and perpendicular to the photodiode probe), and by equivalent cross-sectional area diameter. The four different particle habits identified were circles, needles, dendrites and irregular shapes. Using this information, three different schemes were used to derive the IWC.

The first scheme is based on the Brown and Francis (1995) approach, assuming D_{ij} in Equation (2a) is a mean maximum length. In this scheme, the coefficients a and b in Equation (2a) correspond to the habit $j = 1$, which are aggregates of unrimmed plates, side planes, bullets and columns (Locatelli and Hobbs, 1974). The IWC derived from this scheme is represented by IWC_{BF}.

The second method is based on Equation (2b), using Cunningham (1978) coefficients and is represented by IWC_C. In this scheme, particles are categorized into three groups, aggregates, dendrites and needles, based on coefficients provided by Cunningham (1978). For irregular and circular-shaped particles, however, *Cunningham* coefficients for aggregates of plates and dendrites were used.

The third scheme, which is represented by IWC_M, is based on coefficients provided by Mitchell *et al.* (1990). In this scheme, irregular, circular and dendrite particles are represented by the Mitchell *et al.* (1990) coefficients for aggregates of side planes, bullets and columns. Mitchell *et al.* (1990) also provided a coefficient for needles. The coefficients used in all the schemes are given in Table 1. For this analysis, particle sizes from 125 to 575 μm (from PMS 2D-C) and 600 μm and up (from PMS 2D-P) measurements have been used.

3.2. Comparison of derived IWCs with direct measurements

The derived IWC from the three schemes using data from all four projects were plotted against the IWC measured with a Nevzorov TWC probe (IWC_{Nev}), and this is shown in Figure 1. The derived IWC from the

Table I. The coefficients (a and b) used for different particle habits. IWC_M, IWC_C, and IWC_{BF} are the IWCs derived from the three schemes as defined in the text

$M = aD^b$	D (mm); M (mg)
IWC_M	Needle $a = 0.0049$; $b = 1.8$
	Irregular $a = 0.022$; $b = 2.1$
	Dendrite $a = 0.022$; $b = 2.1$
	Circles $a = 0.022$; $b = 2.1$
$D_e = aA^b$	A (mm^2); D_e (mm)
IWC_C	Irregular $a = 0.39$; $b = 0.31$; $A \leq 0.25$ mm^2
	$a = 0.44$; $b = 0.4$; $A > 0.25$mm^2
	Circles like the irregular
	Needle $a = 0.42$; $b = 0.35$
	Dendrite $a = 0.39$; $b = 0.31$; $A \leq 1.07$mm^2
	$a = 0.38$; $b = 0.48$; $A > 1.07$mm^2
$M = aD^b$	D(μm); M (g)
IWC_{BF}	All shapes (as irregular)
	$a = 7.38 \times 10^{-11}$; $b = 1.9$; $D \geq 100$ μm
	$a = 4.82 \times 10^{-13}$; $b = 3$; $D < 100$ μm

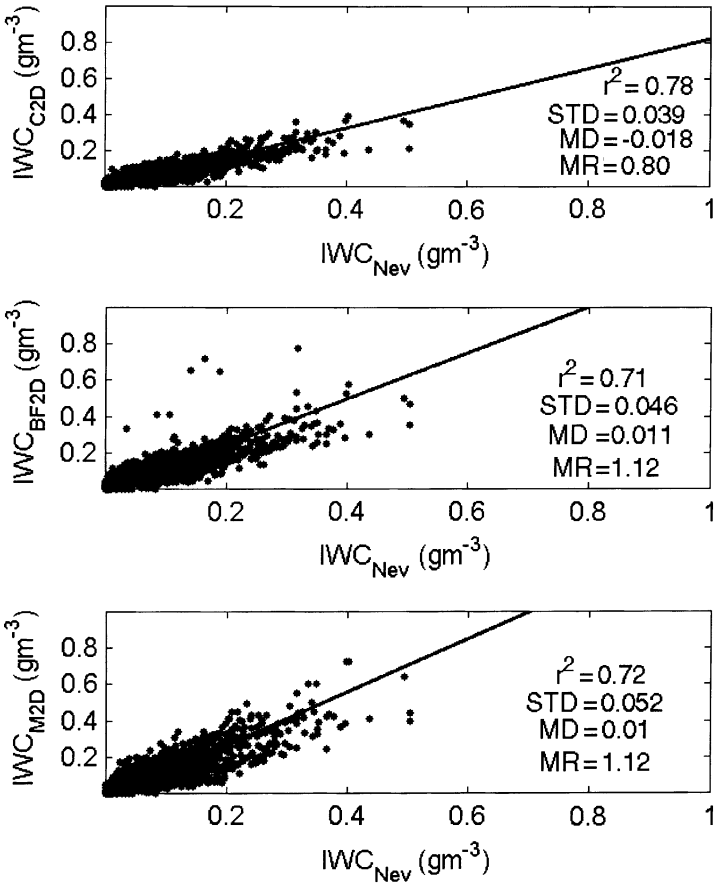

Figure 1. The derived IWCs from the three schemes using 2D-C and 2D-P spectra obtained during all projects verses the measured IWC (IWC_{Nev}). STD, mean difference (MD), coefficient of determination r^2 and mean ratio (MR) are also given

IWC_C scheme shows a good correlation with the measured IWC_{Nev} with a coefficient of determination r^2 near 0.8. The correlation coefficient for the other two schemes, IWC_{BF} and IWC_M, are slightly smaller and near 0.7. The mean ratio ($MR = (\overline{IWC}/\overline{IWC}_{Nev})$) calculated for IWC_C is 0.8. This is consistent, because small particles were not included in the calculation. On the other hand, the mean ratios calculated for the other two schemes were 1.12 (bottom two panels); thus, both these methods overestimated the mass compared with the direct measurements. On some occasions, the calculated IWC from these two schemes reached 0.6–0.8 g m^{-3}, which was not observed in *in-situ* measurements. When small particles were included, as will be discussed later, the ratio for these two schemes became even larger, overpredicting the mass by more than 32% compared with the *in-situ* measurements.

4. CONSIDERING SMALL PARTICLES BY USING THE FSSP AND 2D-C PROBE

Small ice crystals can be important for both solar and thermal infrared (IR) radiative transfer (Platt *et al.*, 1989; Kinne *et al.*, 1992). If they occur in sufficient abundance compared with large crystals, then small ice particles can significantly alter the radiative properties of ice clouds (Arnott *et al.*, 1994). In cirrus cloud over the tropical Pacific, Heymsfield and MacFarquhar (1996) found that small particles make up more than 50% of the mass and are responsible for more than 50% of the extinction in the upper colder parts of cirrus. However, in the lower warmer region, they found that large ice crystals dominated the cloud and small particles were only responsible for 10% of the extinction.

To study the effects of small particles in the parameterization, small particles are included by using a gamma distribution function in the form:

$$n(D) = \kappa D^{\alpha} \exp(-\delta D) \tag{3}$$

where $n(D)$ is the particle distribution with equivalent projected area diameter, $\alpha = 2$, and κ and δ are some constants that are obtained from measured data as described below. Since instruments that can measure small particles with a reliable accuracy are not available, the actual values of the parameters given in Equation (3) are not well known. As a result, various forms of Equation (3) have been used to describe small ice particles (Mitchell and Arnott, 1994; MacFarquhar and Heymsfield, 1997; Wyser, 1998). For example, MacFarquhar and Heymsfield (1997) assumed $\alpha = 1$ to describe the ice particle distribution with mass equivalent diameters <100 μm. Wyser (1998) suggested that $\alpha = 3$ gives the best results for small ice particle spectra with maximum diameters ≤ 20 μm. For the results presented here, the primary assumption was that the FSSP gives a reliable estimation of total ice particle concentration. Therefore, integration of Equation (3) should match the total concentration measured by the FSSP. The other condition that should be satisfied is that the 2D-C spectra and the spectra predicted by Equation (3) should match at 125 μm. Equation (3) is integrated analytically with integration limits of 3 to 92 μm. These integration limits are chosen because of the fact that the FSSP measures particle sizes between the two limits. The values of κ and δ were predicted using 2D-C spectra at 125 μm and the concentration measured by the FSSP (see Appendix A for more discussions). Figure 2 shows the frequency distribution of δ, which exhibited very little variation and had an average value of 0.11 $(\mu m)^{-1}$ and standard deviation (STD) of 0.0014 $(\mu m)^{-1}$. The value of κ, however, varied considerably, with an average value of 1.13×10^3 $(\mu m)^{-3}$ m^{-3} and an STD of 1.05×10^3 $(\mu m)^{-3}$ m^{-3}. This variation of κ was correlated ($r^2 = 0.89$) with IWC derived using small particles, but temperature seems to have no significant effect on κ. The shape of the equation used here is arbitrary, but, as will be shown later, the equation works reasonably well when compared with direct measurements. After determination of the coefficients in Equation (3) for given spectra, the IWC associated with small particles ($D \leq 100$ μm), which is defined as IWC_G, and their projected area per unit volume A_{cG} are derived using equations of the form:

$$IWC_G = \frac{\pi}{6}\rho_{ice}\int_3^{100} D^3 n(D)\,dD \qquad (g\ m^{-3})$$

$$A_{cG} = \frac{\pi}{4}\int_3^{100} D^2 n(D) dD \qquad (\mu m^2\ m^{-3}) \tag{4}$$

where D (μm) is the diameter of the equivalent cross-sectional area of a sphere, and ρ_{ice} is the density of ice and set at 0.78×10^{-12} g μm^{-3} (Heymsfield, 1972).

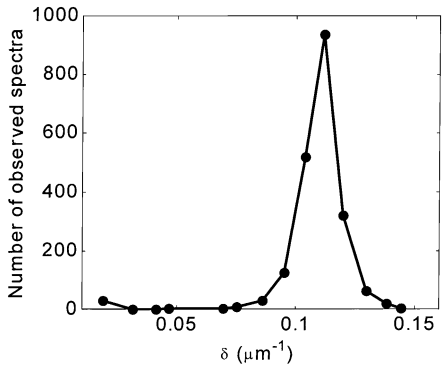

Figure 2. The frequency distribution of δ for all the data

The IWC derived from the gamma distribution function alone is represented by IWC_G. The IWCs derived from 2D spectra plus the gamma distribution are represented by IWC_{C2DG}, IWC_{BF2DG}, and IWC_{M2DG} corresponding to the schemes of IWC_C, IWC_{BF}, and IWC_M respectively. Figure 3 shows a plot of the ratio IWC_G/IWC_{C2DG} against IWC_{C2DG}. The contribution of small particles ($D \leq 100$ μm) increases, on average, with decreasing IWC, suggesting that small particles contribute more to the total mass at lower IWC. The calculated mean ratio was 0.20, implying that, on average, small particles contribute to the total mass by about 20%.

Figure 4 shows the ratio A_{cG}/A_{c2DG} plotted against the total calculated projected area per unit volume (A_{c2DG}). As with the mass, the ratio, on average, decreases with increasing area. The contribution of small

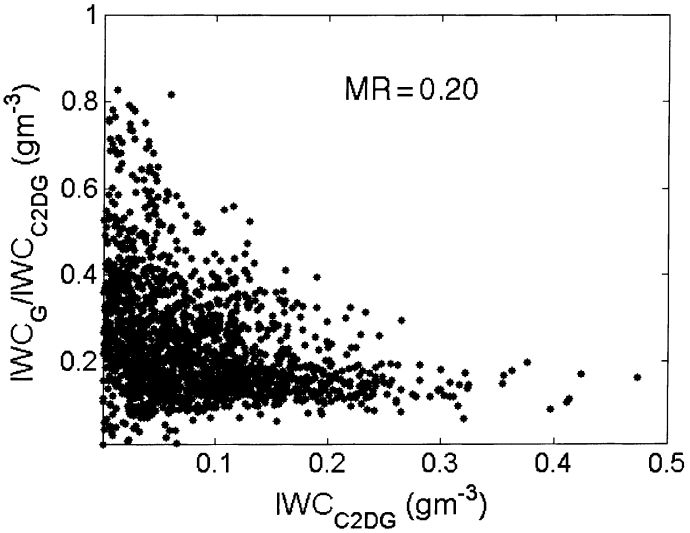

Figure 3. The ratios of estimated mass of small particles ($D \leq 100$ μm) with gamma distribution function (IWC_G) to the IWC_{C2DG} plotted against IWC_{C2DG}

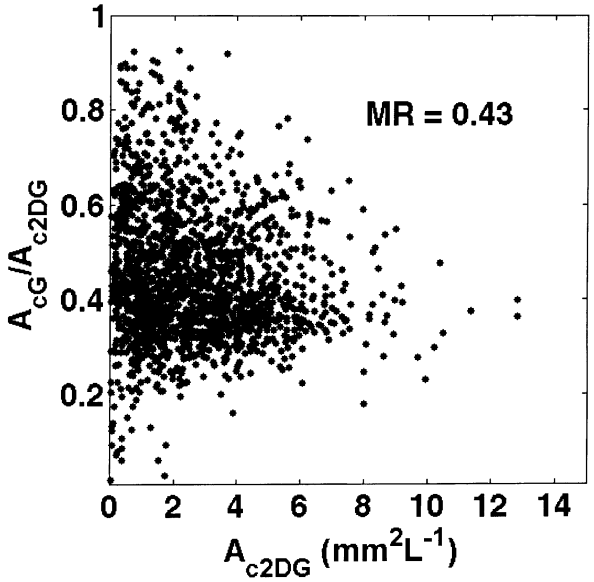

Figure 4. The ratios of estimated total projected area per unit volume of small particles ($D \leq 100$ μm) with gamma distribution function A_{cG} to the A_{c2DG} plotted against A_{c2D}

particles to the total projected area per unit volume is found to be large than the mass with a mean ratio of 0.43.

In order to validate the consideration of small particles, the derived IWCs are plotted against the IWC_{Nev} as shown in Figure 5. The mean ratio MR = $\overline{(IWC_{2D} + IWC_G)}/\overline{IWC_{Nev}}$, STD, the mean difference (MD) $\overline{(IWC_{2D} + IWC_G) - IWC_{Nev}}$, and coefficients of determination r^2 are also shown in Figure 5. The r^2 calculated for IWC_{C2DG} (top panel) was about 0.8, which is similar to the case when only the 2D spectra were used (see Figure 1). The r^2 values for the other two cases (bottom two panels) are also similar to Figure 1, with a slight increase for IWC_{M2DG} (bottom panel). As shown in Figure 5, the Cuningham coefficients gave remarkably close values to the direct measurements with MR of 0.99, STD of 0.037 and MD of −0.001. The other two schemes overestimate the *in-situ* measurements on average by ∼32% and the MD for both cases was 0.028. The results, particularly using Cunningham coefficients, suggest that the IWC_G values estimated by the gamma distribution function are very reasonable.

It is also worth noting that using the Cunningham coefficient for aggregates for all particles, which is not shown here, gave very similar results to the IWC_C scheme. This is because most of the mass is dominated by irregular particles, which is consistent with the observation made by Korolev *et al.* (1999). The three other habits (circles, needles and dendrites) contributed <20% of the total mass. This suggests that assuming all particles are aggregates (which most closely resemble irregular particles) may give a reasonable estimate of the mass. The observed difference between the IWC_C and the other two may not be totally related to the particle habit treated in the calculation of the IWCs. The difference may be partially attributed to the way that particles are categorized and measured. As mentioned earlier, the projected area of a particle is known with

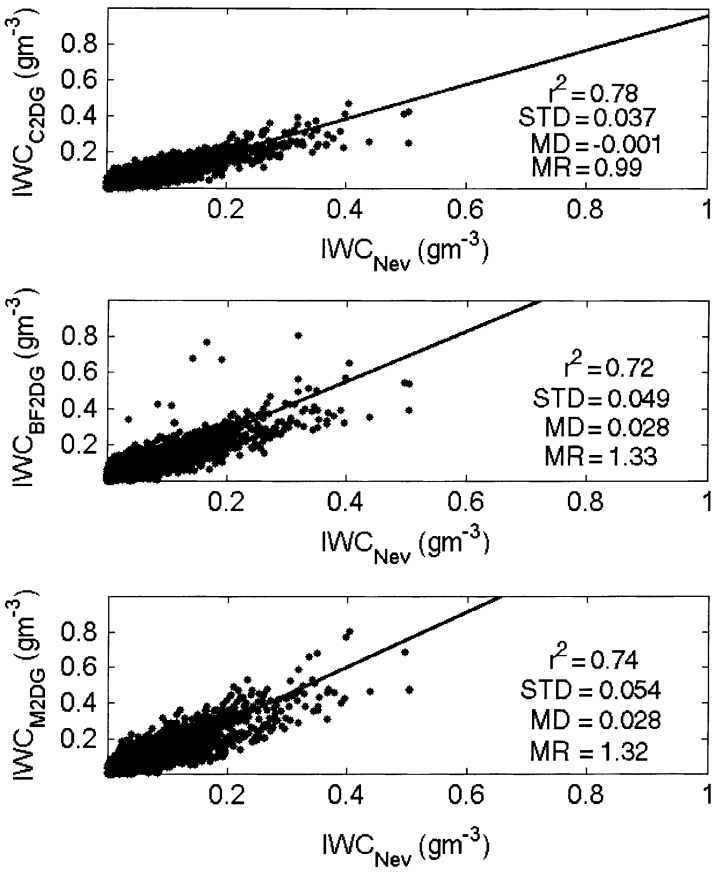

Figure 5. The derived IWCs from the three schemes using 2D-C and 2D-P spectra and from a gamma distribution function fitted to the FSSP concentrations obtained during all projects are plotted against the measured IWC (IWC_{Nev})

much more accuracy than the size, since it can be determined without some assumption of the particle habit. As a result, the mass of a particle predicted using its projected area may be much more accurate than its length. This may be the reason why the Cunningham coefficients gave a better result than the other schemes when they are compared with the direct measurements. In the following we will use the IWC_C scheme to determine IWC from 2D-C and 2D-P measurements.

5. PARAMETERIZATION OF THE IWC WITH TEMPERATURE

IWC has been parameterized in terms of temperature for cirrus clouds (Stephens *et al*., 1990). They have shown that the IWC increases exponentially with temperature. In order to assess the temperature dependence of the IWC, the IWC derived with and without small particles are averaged for every 2 °C interval. These averaged IWCs are represented by IWC_1 and IWC_2 corresponding to without and with small particles respectively, and the results are given in Tables II and III. Following Stephens *et al*. (1990), the mean IWC given in Table II are fitted with mean temperature T using an exponential functions as:

$$\begin{bmatrix} IWC_{1T} \\ IWC_{2T} \end{bmatrix} = q \exp(\eta T) \begin{bmatrix} \eta = 0.054,\ q = 0.114;\ \text{without small particles} \\ \eta = 0.038,\ q = 0.124;\ \text{with small particles} \end{bmatrix} \tag{5}$$

where η and q are some constants obtained from the data fitting. Here T is in centigrade. Figure 6 shows the IWC_1 (panel A) and IWC_2 (panel B) plotted against the mean temperature. The IWC generally increase with temperature. This is consistent with other observations (Stephens *et al*., 1990; MacFarquhar and Heymsfield, 1997). The value of η (0.04) found by Stephens *et al*. (1990) is very close to the value found in this work when the small particles were included, but the value of q found here is higher by at least an order of magnitude. The difference may be attributed to the fact that, in this work, all stratiform ice clouds, including cirrus, were analysed, and they are generally characterized by more mass and total cross-sectional area A of

Table II. The mean D_{ge} (D_{ge1}) and IWC (IWC_1) without including small particles calculated for 2 °C temperature intervals. The STDs, mean temperature T and the number of averaged points are also given

D_{ge1} (μm)	D_{ge1} STD	IWC_1 (g m^{-3})	IWC_1 STD	T (°C)	No. of points
63.462	7.009	0.074	0.054	−1.166	79
63.337	6.907	0.092	0.061	−3.272	194
60.755	8.544	0.087	0.056	−5.056	267
57.356	6.588	0.087	0.059	−7.066	311
57.835	7.813	0.084	0.060	−8.863	128
59.383	8.218	0.073	0.058	−11.117	190
51.682	5.333	0.064	0.050	−13.200	272
48.420	3.572	0.050	0.058	−15.084	97
48.455	3.586	0.056	0.044	−16.764	127
46.594	1.782	0.025	0.036	−19.148	134
46.756	1.709	0.028	0.030	−20.864	68
46.193	2.048	0.045	0.058	−22.964	44
46.230	1.047	0.042	0.036	−24.964	14
46.166	0.881	0.031	0.034	−27.231	44
46.391	0.787	0.035	0.034	−28.875	31
47.033	1.053	0.014	0.007	−30.551	8
47.470	0.814	0.023	0.016	−33.157	39
47.258	0.775	0.016	0.013	−35.203	4
47.840	1.127	0.019	0.022	−37.146	5
48.721	0.477	0.009	0.006	−38.985	4

Table III. The mean D_{ge} (D_{ge2}) and IWC (IWC_2) including small particles calculated for 2 °C temperature intervals. The STDs, temperature T and the number of averaged points are also given

D_{ge2} (μm)	D_{ge} STD	IWC_2 (g m^{-3})	IWC_2 STD	T (°C)	No. of points
42.865	7.948	0.093	0.064	−1.166	79
45.527	6.603	0.113	0.071	−3.272	194
44.681	7.080	0.106	0.066	−5.056	267
42.429	6.257	0.105	0.068	−7.066	311
42.774	7.532	0.101	0.069	−8.863	128
43.301	8.604	0.088	0.066	−11.117	190
37.267	5.400	0.082	0.059	−13.200	272
35.999	4.722	0.064	0.068	−15.084	97
38.045	8.431	0.071	0.055	−16.764	127
33.031	3.722	0.035	0.0445	−19.148	134
32.015	4.832	0.042	0.039	−20.864	68
30.692	3.604	0.067	0.069	−22.964	44
30.140	5.574	0.069	0.049	−24.964	14
30.883	5.325	0.050	0.051	−27.231	44
29.634	1.921	0.060	0.054	−28.875	31
29.886	1.472	0.026	0.018	−30.551	8
30.829	3.882	0.041	0.0263	−33.157	39
26.964	2.236	0.033	0.022	−35.203	4
27.590	4.678	0.031	0.029	−37.146	5
27.292	1.698	0.022	0.0170	−38.985	4

ice crystals compared with cirrus cloud. Their parameterization was based on limited cirrus data published by Heymsfield and Platt (1984). It should also be noted that there are considerable errors associated with averaging the IWC, as indicated by the STDs. In Figure 6, however, the coefficients given in Equation (5) capture most of the variability of the mean IWC with temperature with coefficient of determination r^2 near to 0.8 (panels A and B).

6. PARAMETERIZATION OF THE MEAN EFFECTIVE SIZE WITH TEMPERATURE AND THE IWC

6.1. Derivation of the mean effective size using 2D (2D-C and 2D-P) spectra

The mean effective size of ice crystals ($D > 100$ μm) is calculated following Fu (1996) as:

$$D_{ge2D} = \frac{2(3)^{1/2} IWC_{2D}}{3\rho_{ice} A_{c2D}} \tag{6}$$

where A_{c2D} is the total cross-sectional area of ice particles per unit volume as measured by 2D probes, IWC_{2D} is the IWC determined from 2D spectra using one of the three schemes mentioned earlier, and ρ_{ice} is the density of pure ice (0.9167 g cm^{-3}). The choice of density for pure ice is consistent with a refractive index used in the SSP parameterization scheme described in Fu (1996). Defining the effective size for ice crystals by Equation (6) is necessary for light scattering and absorption studies, because in this form both IWC and total projected area are preserved, and both quantities are important for radiative transfer calculations (Fu, 1996; Fu *et al.*, 1998). Similar, but not identical, definitions of effective ice crystal size were used by Foot (1988) and Francis *et al.* (1998). The total projected area of ice crystals ($D > 100$ μm) per unit volume for each 30 s averaged data is calculated as:

$$A_{c2D} = \sum_{ij} N_{ij} A_{ij} \tag{7}$$

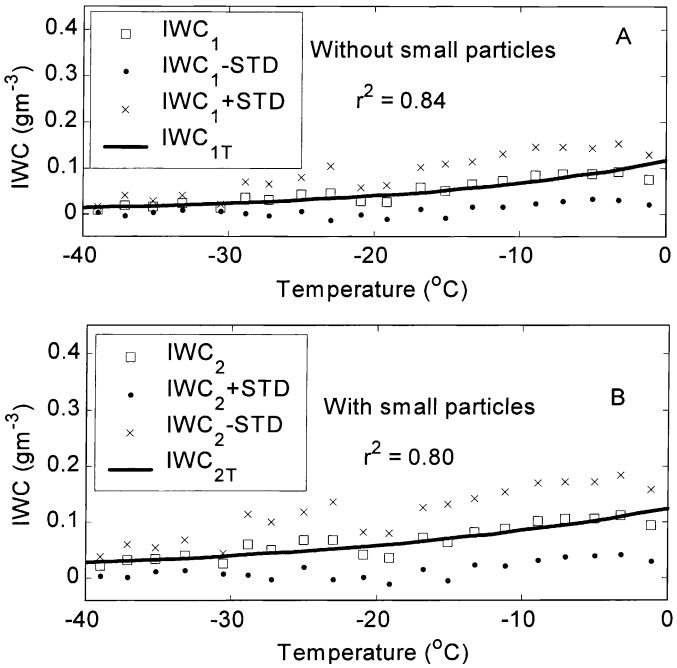

Figure 6. The average IWC after (IWC_2) and before (IWC_1) corrections for small particles, plotted against the temperature. The STD and coefficient of determination are also shown

where N_{ij} is the particle distribution with respect to equivalent area diameter for bin size i and habit j, and A_{ij} is the projected area, as measured by 2D probes. For a given particle i, A_{ij} represents a number of pixels of the 2D image and it is known with better accuracy than D, independent of particle habit. Each pixel that forms a 2D image is represented by a square for any particle shape; thus, the area of a given pixel is simply 625 μm^2 for the 2D-C probe and 4×10^4 μm^2 for the 2D-P probe. The contribution of small particles to D_{ge} is considered using Equation (4).

6.2. *Parameterization of* D_{ge} *based on 2D spectra without including small particles*

In order to assess the average effective size of ice particles in high-latitude clouds, the 30 s averaged data collected during the four projects were averaged for each 2 °C interval and the STDs were calculated as discussed earlier. The averaged D_{ge2D} is represented by D_{ge1}, and the results are given in Table II. Figure 7 shows the plot of D_{ge1} against temperature. The correlation of D_{ge1} with temperature ($r^2 = 0.67$) is relatively lower than with IWC. The D_{ge1} increases with temperature for temperatures -20 °C, but at colder temperatures it shows a slight decrease with temperature. As will be discussed later, the decreasing trend of D_{ge1} with increasing temperature is mainly caused by the absence of small particles. The STDs, on average, increase with temperature. The best-fit line is given by the function:

$$D_{ge1T} = 60.075 \ \exp(0.008T) \tag{8}$$

where the temperature T is in centigrade. It is evident that D_{ge1T} does not fit the D_{ge1} that well. Since D_{ge} also depends on IWC, it is reasonable to consider a parameterization of D_{ge} in terms of both IWC and temperature. Note also from Equation (6) that D_{ge} is related to the projected area per unit volume A_c. It has been shown by Heymsfield and MacFarquhar (1996) that A_c can be described as $a\text{IWC}^b$. Thus, in order to capture the variability of D_{ge} better, as shown in Figure 7, D_{ge} is parameterized as:

$$D_{ge1E} = \alpha_1 \text{IWC}^{\alpha_2} \exp(\alpha_3 T) \ (\mu m) \tag{9}$$

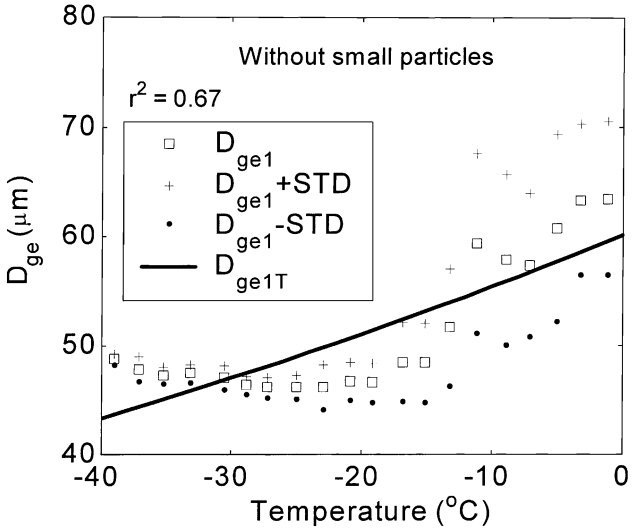

Figure 7. The mean effective size D_{ge1} before corrections for small particles, plotted against the temperature. The STD and coefficient of determination are also shown

where α_1, α_2, and α_3 are some constants obtained from the data fitting, and these constants are calculated to be 57.133, −0.0313, and 0.011 respectively. The IWC and T are given in gm^{-3} and °C respectively. D_{ge1} and D_{ge1E} are well, correlated with $r^2 = 0.71$. However, calculation of D_{ge} using the data in Table II indicates that D_{ge1E} still underestimates the D_{ge1} at cold temperatures.

6.3. Parameterization of D_{ge} *including small particles*

The mean effective sizes D_{ge2DG} are calculated using A_{c2DG} and IWC_{C2DG} in Equation (6). Then the D_{ge2DG} values are averaged as described in Section 6.2 and the results are shown in Table III. The averaged values of IWC_{C2DG} and D_{ge2DG} are represented by IWC_2 and D_{ge2} respectively. Similar to Equations (6) and (9), the variability of the average D_{ge} calculated from the data that were corrected for small particles can be described by the expressions:

$$D_{ge2E} = 53.005 \times IWC^{0.06} \exp(0.013T) \tag{10a}$$

or

$$D_{ge2T} = 46.4 \exp(0.015T) \tag{10b}$$

where D_{ge} is in micrometres and T is in centigrade. These expressions agree with D_{ge2} much better than the case when no small particles were considered. When no small particles were considered, note that the coefficient of determination r^2 between estimated D_{ge} from the parameterization (D_{ge1E}) and measured D_{ge} (D_{ge1}) was 0.71, but with small particles the r^2 increased to 0.93 (Figure 8, panel B). When small particles are included, the coefficient of determination of D_{ge} with temperature has also been improved from 0.67 (Figure 4) to 0.92 (Figure 8, panel A). As shown in Figure 8 (panel A), Equation (10b) describes the variations of the averaged D_{ge} with temperature quite well. When small particles are included, D_{ge} increases with temperature. This suggests that the decrease of the averaged D_{ge} with increasing temperature for colder temperatures observed in Figure 7 was due to the absence of small particles. The inclusion of small particles generally causes D_{ge} to be reduced. This is mainly because small particles contribute more to the total projected area than to the total mass by at least a factor of two. D_{ge} varies with temperature and IWC as shown in Figure 9, in which the ratio $(D_{ge1} - D_{ge2})/D_{ge1}$ and IWC_2 are plotted as a function of temperature. The rate of reduction of D_{ge} due to

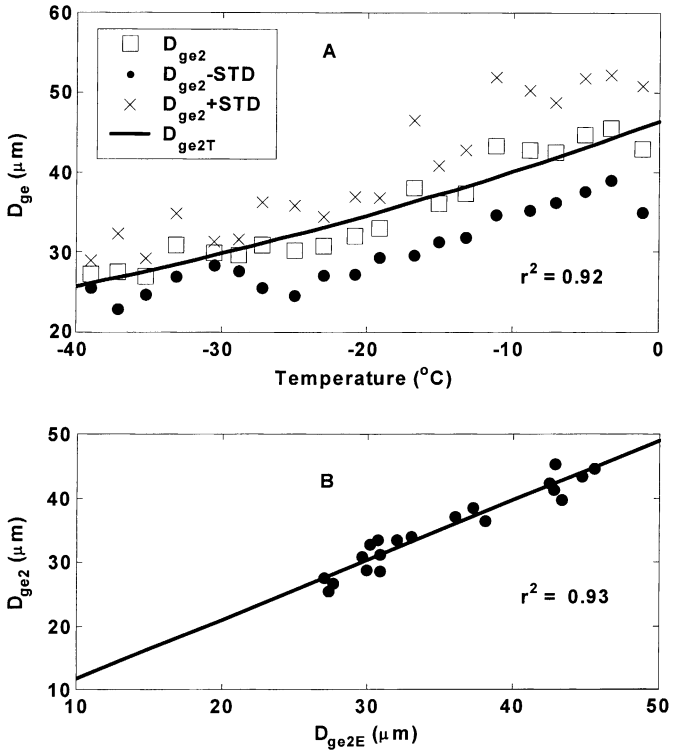

Figure 8. The mean effective size D_{ge2}, after corrections for small particles, is plotted against the temperature (panel A) and D_{ge2} is also plotted with the mean estimated effective size D_{ge2E} (panel B). The STD and coefficient of determination are also shown

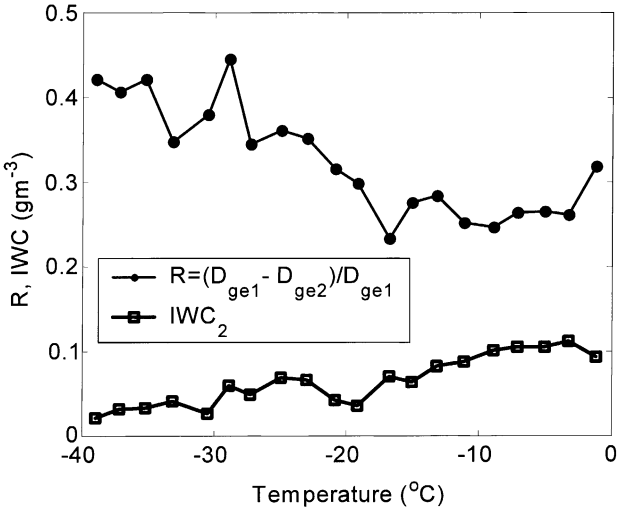

Figure 9. The ratio $(D_{ge1} - D_{ge2})/D_{ge1}$ and the mean IWC (IWC_2) are plotted against temperature

small particles generally increases with both decreasing IWC and temperature, reaching a maximum of 45% at temperatures colder than −25 °C. Thus, neglecting small particles, particularly for cold ice clouds, can result in an overestimation of the effective size by at least 30 to 45%, depending on temperature, and this is consistent with previous observation in cirrus by Francis *et al.* (1998). This overestimation of the effective sizes can

alter the radiative properties of ice clouds, particularly for high-altitude cirrus clouds with temperatures colder than $-30\,^{\circ}$C. Figure 10 shows a plot of estimated D_{ge} (D_{ge2E}) from Equation (10a) as a function of IWC and temperature. At a given temperature, the effective size increases rapidly with the IWC to a certain value, and then it levels off. At the coldest temperature, the effective size seems to approach asymptotically near 30 μm and at the warmest temperature near 55 μm. However, the effective size changes with temperature at a steady rate of $\sim$0.5 μm $^{\circ}$C^{-1}. Similar asymptotic behaviour of D_{ge} to $\sim$116 μm has been reported by MacFarquhar and Heymsfield (1998). This value, however, was an upper bound for the data collected in deep convective outflow anvils of tropical cirrus. This D_{ge} value is significantly higher than the maximum $D_{ge} \approx 65$ μm calculated using 30 s averaged data that was corrected for small particles in this work. MacFarquhar and Heymsfield (1998) also observed similar asymptotic behaviour of D_{ge} to varying values of 31–123 μm when some ice crystal shapes, such as hexagonal plates, crystals with sectorlike branches, and broad-branched crystals, were used to derive IWC using Mitchell (1996) mass to dimensional relationships. Using 2D-C and replicator measurements in cirrus clouds, and a gamma distribution function for small particles, Francis *et al.* (1998) estimated the lower limit of mean effective radius r_e of $\sim$19.7 μm for the highest altitude (near 275 hPa). D_{ge} is related to r_e as $D_{ge} = 1.54 r_e$; thus, this value corresponds to $D_{ge} \approx 30$ μm. It is hard to make direct comparison with this work, since the temperature at which these measurements were made was not reported. This value, however, corresponds to the D_{ge} predicted at a temperature of around $-30\,^{\circ}$C and IWC $\approx$ 0.05 g m^{-3}. The applicability of this result outside the high-latitude stratiform ice clouds may be questionable. However, the result suggests that a possible increase of IWC greater than $\sim$0.06 g m^{-3} with decreasing altitude may not significantly alter the value of D_{ge}, although there may be some effects of temperature on D_{ge}.

The parameterization coefficients α_1, α_2, and α_3 (see Equation (9)) obtained for each project after small particles were included are shown in Table IV, where the data are categorized by project and geographical region. Generally, the three coefficients calculated for CFDE I, CFDE III, and combined CFDE I & CFDE III are very similar. However, α_2 and α_3 calculated for FIRE.ACE and BASE have considerable variations. Nevertheless, the comparisons of the parameterizations given in Table IV indicate that there are no significant regional variations in calculated mean D_{ge}. This is shown in Figure 11, where the parameterized D_{ge2E} values calculated from derived IWC and temperature during the four projects are plotted against temperature. As indicated in Figure 11, all the parameterizations agreed reasonably well, except that the FIRE.ACE and CFDE I data showed some variability at warmer and colder temperatures respectively. This is likely due to the limited number of observed data points in these subsets of the data.

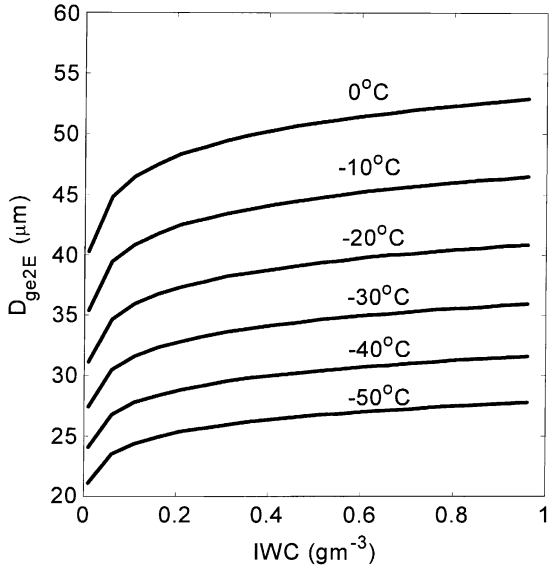

Figure 10. The parameterized D_{ge} (D_{ge2E}) from Equation (10a) plotted against arbitrary IWC and temperature

Table IV. The parameterization coefficients α_1, α_2, and α_3 (see Equation (9)), and coefficients of determination r^2 between parameterized and measured for each project for the data that was corrected for small particles. The data are categorized by project and geographical location

	FIRE.ACE and BASE	CFDE I and CFDE III	FIRE.ACE	BASE	CFDE I	CFDE III
α_1	46.686	66.235	128.0783	43.9289	77.0168	68.6325
α_2	0.0041	0.1456	0.2278	−0.0196	0.2138	0.1622
α_3	0.0139	0.0163	0.0211	0.0149	0.0176	0.0143
r^2	0.84	0.93	0.76	0.78	0.95	0.93

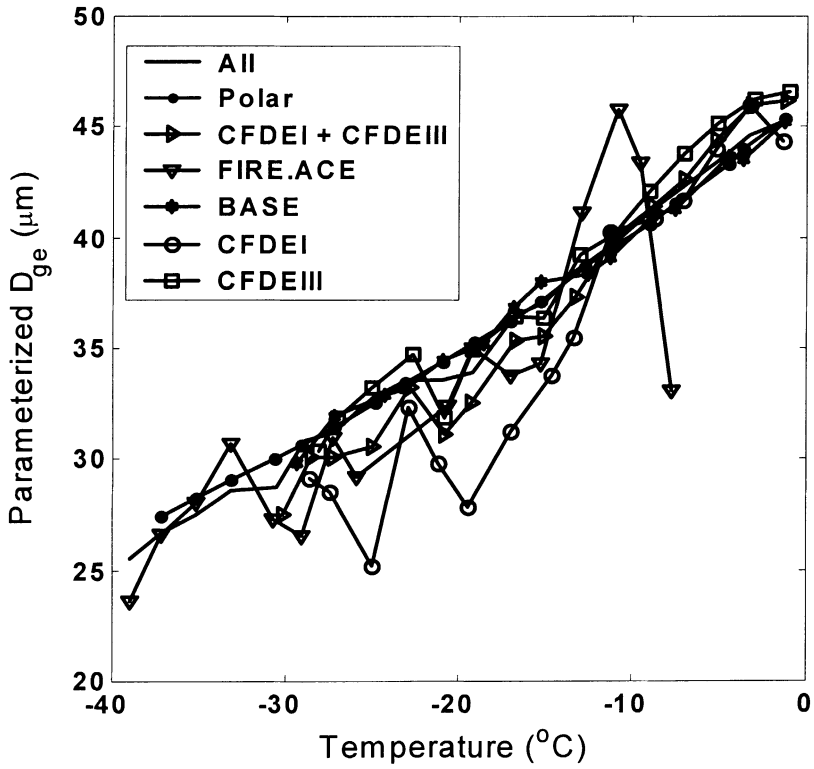

Figure 11. The parameterizations of the average D_{ge} for four projects and two geographical areas, as listed in Table IV. The combined data are also shown. The parameterized D_{ge} values are calculated from the measured IWC and temperature in the given region

7. SUMMARY AND CONCLUSION

Three methods used for deriving IWC from ice particle spectra measured with PMS 2D probes and concentrations using the PMS FSSP have been tested against the IWC measured with the Nevzorov probe in various high-latitude ice clouds. A parameterization of IWC in terms of temperature was obtained with and without small ice particles (Equation (5)). Two parameterizations of mean effective size D_{ge}, one in terms of temperature and IWC (Equations (10a) and (9)), and the other in terms of temperature alone (Equations (10b) and (8)) have been developed. The parameterization given in Equations (10a) and (10b) includes small particles. The IWC was derived using the Cunningham coefficients. The data analysed in this work include Arctic and other clouds covering large areas of western and eastern parts of Canada approximately north of 45 °N with a wide range of measured IWC (0.001 to 0.45 g m^{-3}). The parameterizations are valid for

the average conditions of high-latitude stratiform ice clouds with temperatures between 0 and −40 °C. These parameterizations are mainly intended for use in climate models. Based on the results in this work, it is difficult to make a strong statement about which parameterization, Equation (10a) or (10b), gives a better result. Model sensitivity studies can give some insights about choosing the parameterization that is more suitable for GCM application.

Small particles may contribute significantly to the optical properties of ice clouds. However, the unavailability of an instrument that can accurately measure small particles ($D \leq 100$ μm) has made it difficult for any cloud microphysical parameterizations. As a result of this, concentrations were inferred using an FSSP. The FSSP may overcount ice particles by an unknown factor. However, it probably does not exceed a factor of two. When the small particles were included in the parameterization, the mass predicted using the gamma distribution function fitted to the total concentration measured with FSSP gave a reliable estimate of the mass measured with the Nevzorov probe. So, this is a good test for the applicability of the scheme. However, a more satisfactory test of the parameterization still awaits the availability of suitable instruments for measuring small particles. This parameterization, however, is unique compared with the other methods, such as that of MacFarquhar and Heymsfield (1997), in the sense that D_{ge} is directly related to temperature. In the MacFarquhar and Heymsfield (1997) scheme, the effective sizes can be derived only for a given temperature interval, and certain assumptions about the particle sizes are also required for integration.

In this work the following conclusions have also been reached:

(1) it has been demonstrated that there are significant differences among the schemes used to derive the IWC from ice particle spectra when compared with the direct measurements (IWC_{Nev});
(2) the IWC derived from the Cunningham coefficients gave good estimates of IWC_{Nev}, particularly when small particles were included;
(3) irregular particles contributed most to the derived IWC, compared with other identified particle habits, and this is consistent with observations (Korolev *et al*., 1999);
(4) based on an analysis using the Cunningham relationship and the gamma distribution function for small particles, the contribution of small particles to the total mass (total area) is estimated to be 20% (43%);
(5) on average, it has been shown that the mean effective size D_{ge} and IWC increase with temperature;
(6) no significant regional variation in the calculated D_{ge} has been observed;
(7) on average, inclusion of small particles caused the D_{ge} to become smaller; however, the rate of reduction of D_{ge} depends on the temperature and IWC. The considerable change in D_{ge} due to small particles normally occurred at the coldest temperature and at low IWC, reaching up to about 45%.

ACKNOWLEDGEMENTS

The authors thank Dr Alexei Korolev for providing some of the Nevzorov LWC and TWC probe data. Funding for this analysis was provided by the Natural Sciences and Engineering Research Council of Canada (NSERC), the Panel on Energy Research and Development (PERD), the Canadian Climate Change Action Fund (CCAF), and the US National Science Foundation under grant OPP-0084259 for SHEBA III.

APPENDIX A: DETERMINATION OF PARAMETERS κ AND δ

The gamma function $n_\alpha(D)$ can be given in the form:

$$n_\alpha(D) = \kappa D^\alpha \quad \mathrm{e}^{-\delta D} \tag{A.1}$$

where the α, δ, and κ are constants that are obtained as described below. The integral I_α of Equation (A.1) can be given in the form:

$$I_\alpha = \int_{D_{\min}}^{D_{\max}} n_\alpha(D)\,\mathrm{d}D = -\kappa \frac{e^{-\delta D}}{\delta^{\alpha+1}}[(\delta D)^\alpha + \alpha(\delta D)^{\alpha-1} + \alpha(\alpha-1)(\delta D)^{\alpha-2} + \ldots + n!]|_{D_{\min}}^{D_{\max}} \tag{A.2}$$

where D_{max} and D_{min} are any arbitrary maximum and minimum length respectively. In this work, D_{max}, D_{min}, and α are taken to be 92 μm, 3 μm, and 2 respectively. Therefore, Equation (A.2) can be written in the form:

$$I_2 = N_{FSSP} = -\kappa \left\{ \frac{e^{-\delta D_{max}}}{\delta^3}[(\delta D_{max})^2 + 2(\delta D_{max}) + 3] - \frac{e^{-\delta D_{min}}}{\delta^3}[(\delta D_{min})^2 + 2(\delta D_{min}) + 3] \right\} \quad (A.3)$$

where N_{FSSP} is the concentration measured with the FSSP. Equation (A.3) has two unknowns: δ and κ. The parameter κ can be determined from Equation (A.1), assuming that the equation should match the spectra measured with the 2D-C at the 125 μm bin size. Thus, the parameter κ can be calculated as:

$$\kappa = \frac{n_2(125)}{(125)^2 e^{-125\delta}} \quad (A.4)$$

After substituting Equation (A.4) in Equation (A.3):

$$N_{FSSP} + \frac{n_2(125)}{(125)^2 e^{-125\delta}} \left\{ \frac{e^{-92\delta}}{\delta^3}[(92)^2\delta^2 + 184\delta + 3] - \frac{e^{-3\delta}}{\delta^3}(9\delta^2 + 6\delta + 3) \right\} = 0 \quad (A.5)$$

The value of δ in Equation (A.5) is numerically evaluated for each 30 s averaged spectrum.

REFERENCES

Arnott WP, Dong Y, Hallett J, Poellot RM. 1994. The role of small crystals of cirrus: a case study, FIRE II, November 22, 1991. *Journal of Geophysical Research* **99**: 1371–1381.

Arnott WP, Mitchell D, Schmitt C, Kingsmill D, Ivanova D, Poellot MR. 2000. Analysis of FSSP performance for measurement of small crystal spectra in cirrus. In *Proceedings 13th International Conference on Clouds and Precipitation*, Reno, N, 14–18 August; 191–193.

Baumgardner D. 1983. Analysis and comparison of five water droplet measuring devices. *Journal of Climate and Applied Meteorology* **22**: 891–910.

Baumgardner D, Spowart M. 1990. Evaluation of forward scattering spectrometer probe. Part III: time response and laser inhomogeneity limitations. *Journal of Atmospheric and Oceanic Technology* **7**: 666–672.

Boer JG, Arpe K, Blackburn M, Deque M, Gates LW, Hart LH, Treut LH, Roeckner E, Sheinin AD, Simmonds I, Smith BNR, Tokioka T, Wetherald TR, Williamson D. 1992. Some results from an intercomparison of climate simulated by 14 atmospheric general circulation models. *Journal of Geophysical Research* **97**: 12 771–12 786.

Brenguier JL. 1989. Coincidence and dead time corrections for particle counters. Part II: high concentration measurements with FSSP. *Journal of Atmospheric and Oceanic Technology* **6**: 585–598.

Brown ARP, Francis PN. 1995. Improved measurements of the ice water content in cirrus using a total-water probe. *Journal of Atmospheric and Oceanic Technology* **12**: 410–414.

Cober SG, Isaac GA, Korolev AV, Strapp JW. 2001. Assessing cloud-phase conditions. *Journal of Applied Meteorology* **40**: 1967–1983.

Cunningham MR. 1978. Analysis of particle spectral data from optical array (PMS) 1D and 2D sensors. In *American Meteorological Society, Fourth Symposium. Meteorological Observation Instruments*, Denver, USA, 10–14 April; 345–350.

Curry JA, Hobbs PV, King MD, Randall DA, Minnis P, Isaac GA, Pinto JO, Uttal T, Bucholtz A, Cripe DG, Gerber H, Fairall CW, Garrett TJ, Hudson J, Intrieri JM, Jakob C, Jensen T, Lawson P, Marcotte DL, Nguyen L, Pilewskie P, Rangno A, Rogers D, Strawbridge KB, Valero FPJ, Williams AG, Wylie D. 2000. FIRE Arctic clouds experiment. *Bulletin of the American Meteorological Society* **81**: 5–29.

Foot JS. 1988. Some observations of optical properties of clouds: II: cirrus. *Quarterly Journal of the Royal Meteorological Society* **114**: 145–164.

Francis PN, Hignett P, Macke A. 1998. The retrieval of cirrus cloud properties from aircraft multi-spectral reflectance measurements during EUCREX'93. *Quarterly Journal of the Royal Meteorological Society* **124**: 1273–1291.

Fu Q, Yang P, Sun BW. 1998. An accurate parameterization of the infrared radiative properties of cirrus clouds of climate models. *Journal of Climate* **11**: 2223–2237.

Fu Q. 1996. The accurate parameterization of the solar radiative properties of cirrus clouds for climate models. *Journal of Climate* **9**: 2058–2082.

Gardiner BA, Hallett J. 1985. Degradation of in cloud forward scattering spectrometer probe measurements in presence of ice particles. *Journal of Atmospheric and Oceanic Technology* **13**: 1152–1165.

Gultepe I, Isaac GA, Hudak D, Nissen R, Strapp JW. 2000. Dynamical and microphysical characteristics of Arctic clouds during BASE. *Journal of Climate* **13**: 1225–1254.

Gultepe I, Isaac GA, Cober SG. 2001. Ice crystal number concentration versus temperature. *International Journal of Climatology* **21**: 1281–1302.

Heymsfield AJ. 1972. Ice crystals terminal velocities. *Journal of the Atmospheric Sciences* **26**: 1348–1351.

Heymsfield AJ, Parrish JL. 1978. A computational technique for increasing effective sampling volume of the PMS two dimensional particle size spectrometer. *Journal of Applied Meteorology* **17**: 1566–1572.
Heymsfield AJ, McFarquhar MG. 1996. High albedos of cirrus in the tropical Pacific warm pool: microphysical interpretations from CEPEX from Kwajalein, Marshall Islands. *Journal of the Atmospheric Sciences* **53**: 2424–2551.
Heymsfield AJ, Platt CMR. 1984. Parameterization of particle size spectrum of ice clouds in terms of ambient temperature and ice water content. *Journal of the Atmospheric Sciences* **41**: 846–855.
Hudak DR, List R, Krauss T. 1996. Microphysical properties of Arctic cyclones. In *12th International Conference on Clouds and Precipitation*, American Meteorological Society, Boston; 158–161.
Isaac GA, Cober SG, Strapp JW, Korolev AV, Tremblay A, Marcotte DL. 2001. Recent Canadian research on aircraft in-flight icing. *Canadian Aeronautics and Space Journal* **47**(3): 213–221.
Kinne S, Ackerman PT, Heymsfield JA, Valero JPF, Sassen K, Spinhirne DJ. 1992. Cirrus microphysics and radiative transfer: cloud field study on 28 October 1986. *Monthly Weather Review* **120**: 661–684.
Knollenberg RG. 1970. The optical array: an alternative to scattering or extinction for airborne particle size determination. *Journal of Applied Meteorology* **9**: 86–103.
Korolev AV, Strapp WJ, Isaac GA. 1998a. Evaluation of accuracy of PMS optical array probe. *Journal of Atmospheric and Oceanic Technology* **15**: 708–720.
Korolev AV, Strapp WJ, Isaac GA. 1998b. The Nevzorov airborne hot wire LWC–TWC probe: principle of operation and performance. *Journal of Atmospheric and Oceanic Technology* **15**: 1495–1510.
Korolev AV, Isaac GA, Hallett J. 1999. Ice particle habits in Arctic clouds. *Geophysical Research Letters* **26**: 1299–1302.
Locatelli JD, Hobbs PV. 1974. Fall speeds and masses of solid precipitation particles. *Journal of Geophysical Research* **79**: 2185–2197.
McFarquhar GM, Heymsfield AJ. 1997. Parameterization of tropical cirrus ice crystal size distribution and implication for radiative transfer: results from CEPEX. *Journal of the Atmospheric Sciences* **54**: 2187–2200.
McFarquhar GM, Heymsfield AJ. 1998. The definition and significance of effective radius for ice clouds. *Journal of the Atmospheric Sciences* **55**: 2039–2052.
Mitchell DL. 1996. Use of mass–and area–dimensional power laws for determining precipitation particle and terminal velocity. *Journal of the Atmospheric Sciences* **53**: 1710–1723.
Mitchell DL, Arnott. PW. 1994. A model predicting the evolution of ice particle size spectra and radiative properties of cirrus clouds. Part II: dependence of absorption and extinction on ice crystal morphology. *Journal of the Atmospheric Sciences* **51**: 817–832.
Mitchell DL, Zhang R, Pitter R. 1990. Mass–dimensional relationship for ice particles and the influence of riming on snowfall rates. *Journal of Applied Meteorology* **29**: 153–163.
Platt CMR, Spinhirne DJ, Hart DW. 1989. Optical and microphysical properties of cold cirrus cloud: evidence for regions of small ice particles. *Journal of Geophysical Research* **94**: 11 151–11 164.
Ramanathan V, Pitcher J, Malone RC, Blackmon ML. 1983. The response of a spectral general circulation to refinements in radiative processes. *Journal of the Atmospheric Sciences* **40**: 605–630.
Ramaswamy V, Ramanathan V. 1989. Solar absorption by cirrus clouds and the tropical upper troposphere thermal structure. *Journal of the Atmospheric Sciences* **40**: 605–630.
Stephens GL, Tsay SC, Stackhouse PW, Flatau PJ. 1990. Relevance of micro-physical and radiative properties of cirrus clouds to climate and climatic feedback. *Journal of the Atmospheric Sciences* **47**: 1742–1753.
Strapp JW, Chow P, Maltby M, Bezer AD, Korolev AV, Stromberg I, Hallett J. 1999. Cloud microphysical measurements in thunderstorm outflow regions during Allied /BAE 1997 flight trials. In *AIAA 37th Aerospace Science Meeting and Exhibit*, Reno N; 11–14.
Sun Z, Shine KP. 1994. Studies of the radiative properties of ice and mixed phase clouds. *Quarterly Journal of the Royal Meteorological Society* **120**: 111–137.
Wendisch M, Keil A, Korolev AV. 1996. FSSP characterization with monodisperse water droplets. *Journal of Atmospheric and Oceanic Technology* **13**: 1152–1165.
Wyser K. 1998. The effective radius in ice clouds. *Journal of Climate* **11**: 1793–1802.
Yang P, Liou NK. 1996a. Geometric optics integral equation method for light scattering by no spherical ice crystals. *Applied Optics* **35**: 6568–6584.
Yang P, Liou NK. 1996b. Finite element time domain method for light scattering by small ice crystals in three dimensional space. *Journal of the Optical Society of America A: Optics Image Science and Vision* **13A**: 2072–2085.

